Sixth International Symposium on Marine Propulsors
smp'19, Rome, Italy, May 2019

A 3D Flow Separation Model for Open Propellers with Blunt Trailing Edges

Weikang Du[1,*], Spyros A. Kinnas[1]

[1]Ocean Engineering Group, Department of Civil, Architecture and Environmental Engineering, University of Texas at Austin, Austin, Texas, USA

ABSTRACT

The panel method is widely used in the design stage of marine propellers. However, this method cannot handle propellers with blunt trailing edges due to lack of proper models for the flow separation downstream. In this study, a numerical scheme is proposed to predict the flow separation by representing it with an extension. The criteria of zero local lifts and zero local moments are used to establish the equations to determine the shape of the extension, which is solved either by a Newton-Secant method or as an optimization problem. A low-order panel method coupled with a boundary layer solver (the viscous/inviscid interaction method) is used to predict the pressure distributions for the extended geometry. To validate this model, the pressure distributions on the propeller blades are compared with those from the Reynolds-Averaged Navier-Stokes method. The predicted open water characteristics are compared with the experimental measurements. This model requires much less computational effort while preserving high accuracy, and thus can be used reliably in designing and analyzing propellers with blunt trailing edges.

Keywords

Flow separation, propellers with blunt trailing edges, panel method, viscous/inviscid interaction method.

1 INTRODUCTION

The Boundary Element Method (BEM, or more commonly known as the panel method) has been widely used to predict the inviscid flows around propellers due to its high efficiency and acceptable accuracy. The effect of viscosity can be taken into account either via empirical skin frictions, known as the viscous pitch correction (Kerwin and Lee, 1978), or via coupling the BEM with boundary layer solvers, known as the viscous/inviscid interaction (VII) method (Drela, 1989; Milewski, 1997; Hufford et al., 1994; Sun and Kinnas, 2008; Kinnas et al., 2012). While both of these two methods improve the correlation of predicted open water characteristics with experimental measurements, the pressure distributions from VII method are more accurate, especially near the trailing edge (Kim et al., 2018; Du and Kinnas, 2019).

One disadvantage of the panel method or VII method is that they cannot handle the blunt trailing edge (T.E.) sections due to lack of proper models for the flow separation downstream. Propellers with blunt T.E.s are commonly seen, either due to structural reasons or to reduce the high-pitched noise (often referred to as the singing edges). One way to apply the panel method in sections with blunt T.E.s is to reduce the thickness near the T.E.s without changing the camber, as shown in Figure 1. However, this approximation brings in several problems. First, the selection of the point from which modification will start is totally empirical. In Figure 1, the location is selected as 90% of the chord length. Whether this value will affect the predicted thrust and pressure distribution of the propeller requires further justification. Second, in some cases modifying the trailing edge might change the geometry too much, which will affect the accuracy of the panel method. Physically, a more rational approach is to represent the flow separation downstream of the blunt T.E. by an extension.

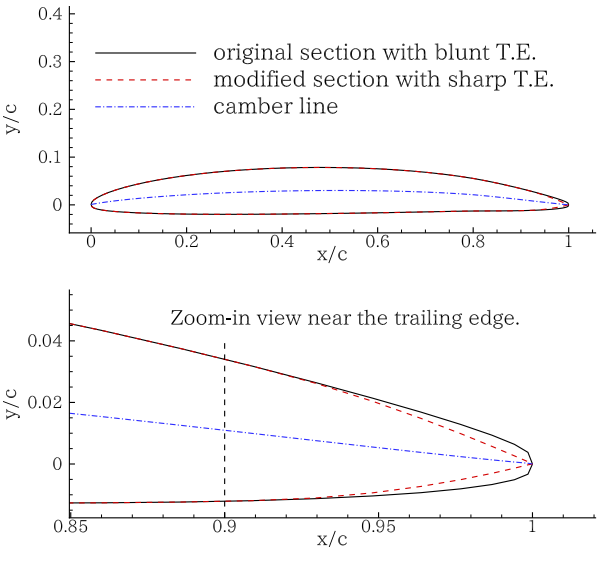

Figure 1: Modify the thickness of a propeller with blunt trailing edge to sharp trailing edge after 90% of the chord length without changing the camber

*Corresponding author, Weikang Du: allendu1988@utexas.edu

Du and Kinnas (2018) developed a flow separation model for hydrofoils and propeller ducts with blunt T.E. sections. This model can be summarized as

- It is assumed that the pressure in the boundary layer separation region is constant*, and this is enforced by the conditions of zero-lift and zero-moment over the extension zone.
- The location of the last point of the extension is determined by the conditions above via a Newton-Secant Method.
- The starting points of the extension on the two sides of the section are determined, in iterative manner, by requiring the friction coefficients to be equal to zero at those points.

It was found that the pressure distributions and skin frictions along the hydrofoils and ducts correlate well with those from the Reynolds-Averaged Navier-Stokes (RANS) method, and the thrust and torque of the ducted propeller agree much better with experimental measurements when the extension is determined from this model, compared to the case where T.E. section is extended to a randomly selected location.

In this paper, Du and Kinnas's (2018) model is extended from two dimensional (2D) to three dimensional (3D) and applied to a 4-blade open propeller with blunt T.E.s. The flow is assumed to be incompressible, fully wetted and steady, i.e., without any cavitation or vortex shedding (only the mean flow is considered). To make some conclusions from the present method applicable to full-scale propellers with blunt T.E.s, the flow is also assumed to be fully turbulent. In the VII method, the laminar-to-turbulent flow transition points are forced at locations 1% of the chord length from the leading edge, and correspondingly, results are compared with those from fully turbulent RANS simulations.

Two assumptions are needed to establish the equations in this model. The first assumption is that *the boundary layer grows mainly in the direction within a strip of a constant radius*, which is the same as in the VII method (Du and Kinnas, 2019). The propeller is cut into strips with constant radii, and then transformed from the cylindrical coordinate system to 2D Cartesian system so that a series of hydrofoils with blunt T.E.s are obtained. Each hydrofoil section is extended to a section with a sharp T.E., and several parameters are used to control the location of the extended T.E. in each section. The extended hydrofoil sections are then transformed back to the cylindrical system to obtain a propeller with a sharp trailing edge.

The second assumption is that *the pressure in the separation region is constant, which leads to the criteria of zero local lifts and zero local moments*. The local lifts and local moments are based on the inviscid pressure distributions, predicted by a low order panel method with a fast wake alignment scheme (PSF-2 type alignment) (Greeley and Kerwin, 1982). The 3D flow separation is represented as an extension, whose shape is predicted by a mathematical model established in this paper, and solved either by a Newton-Secant method or as an optimization problem. After the extension is found within a certain tolerance, the propeller with sharp T.E. is solved by the panel method, which uses a pseudo-unsteady wake alignment scheme (full wake alignment scheme, or FWA) (Tian and Kinnas, 2012) and is coupled with a boundary layer solver to obtain the viscous pressure distributions and forces.

It should be noted that the present method is only applicable to propellers working with a moderate loading and the boundary layer separation is expected to be locally downstream of the blunt trailing edges so that it is physically rational to represent the separation as an extension. The unsteadiness caused by propellers working at extreme off-design conditions where strong flow separation occurs at high angles of attack for some blade sections or due to strong leading edge vortices is beyond the scope of this method. However, as will be shown later in the paper, the predicted forces from the present method agree well with the experimental measurements over a large range of advance ratios.

The pressure distributions on each blade sections and the computational time are compared with full-blown RANS simulations with very fine meshes downstream of the blunt trailing edge to capture the flow separation. The open water characteristics are compared with the experimental measurements, and the computational efficiency of this method is also summarized.

2 METHODOLOGY

2.1 The Reynolds-Averaged Navier-Stokes method

In the RANS method, the velocity field u_i is decomposed into its mean U_i and the fluctuation u_i' (Reynolds, 1894), as

$$u_i = U_i + u_i'. \tag{1}$$

The governing equations in the RANS method are the continuity equation and the momentum equations, as

$$\nabla \cdot \overrightarrow{u} = 0, \tag{2}$$

and

$$\frac{\partial U_i}{\partial t} + U_j \frac{\partial U_i}{\partial x_j} = -\frac{\partial P}{\partial x_i} + \frac{\partial}{\partial x_j}\left(\nu \frac{\partial U_i}{\partial x_j} - \overline{u_i' u_j'}\right), \tag{3}$$

where P = the pressure, ν = the kinematic viscosity; and $\overline{u_i' u_j'}$ = the Reynolds stress.

In this study, the results from the flow separation model are compared with the RANS simulation by using the commercial CFD software STAR-CCM+. The flow is assumed to be steady, incompressible and fully turbulent. In the RANS simulations, the Spalart-Allmaras turbulence model is used (Spalart and Allmaras, 1992), and the

*As indicated by RANS simulations and experiments.

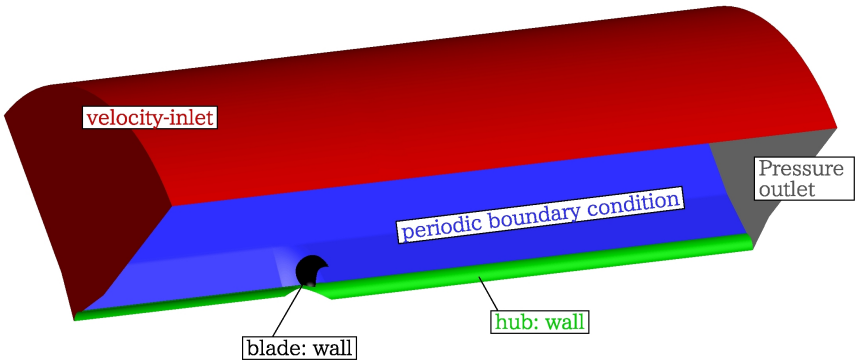

Figure 2: The computational domain and boundary conditions in the RANS simulation

residuals for the continuity and momentum equations are set as 1.0×10^{-6}.

The far-field boundary conditions are velocity inlet and pressure outlet, as shown in Figure 2. Since the inflow is uniform, the periodic boundary condition is used so that only one blade needs to be modeled. The radius of the computational domain is $5R$, where R is the propeller blade radius. The distance from the upstream velocity inlet to the propeller plane is $5.4R$, and the distance from the propeller plane to the pressure outlet is $10.4R$.

In the RANS simulation, polyhedral meshes are used with 30 prism layers to model the boundary layer region. A grid independence study is shown in Table 1, with different numbers of cells used. In this study, The advance ratio is 0.579, which is defined as

$$J_s = \frac{V_s}{nD}, \tag{4}$$

where V_s = the ship speed; n = the propeller rotational frequency; and D = the propeller diameter. The thrust coefficient on the propeller is defined as

$$KT = \frac{T}{\rho n^2 D^4}, \tag{5}$$

and the torque coefficient is defined as

$$KQ = \frac{Q}{\rho n^2 D^5}, \tag{6}$$

where T = the propeller thrust; Q = the propeller torque; and ρ = the fluid density. The differences between the predicted forces in Case 1 and Case 2 are within 0.4%, which shows that the number of cells used in Case 2 is large enough. In this paper, all the results predicted from the RANS simulation are from the meshes used in Case 2.

Table 1: Grid independence study in the RANS simulation ($J_s = 0.579$)

	Number of cells	KT	KQ
Case 1	6.95 million	0.17783	0.02802
Case 2	4.21 million	0.17721	0.02805
Case 3	3.03 million	0.17713	0.02818

To model the flow separation in the RANS method, very fine grids are needed near the blade surface and in the wake region, as shown in Figure 3 and Figure 4. However, O-grids must be used for blade sections with blunt T.E.s, which means that only a short part of the trailing wake can be modeled with fine enough grids, as shown in Figure 4. On the other hand for blade sections with sharp T.E.s C-grids can be used which allow for a longer part of the trailing wake to be modeled with fine grids. In other words, the results of RANS simulations for propellers with blunt T.E.s might not be as reliable.

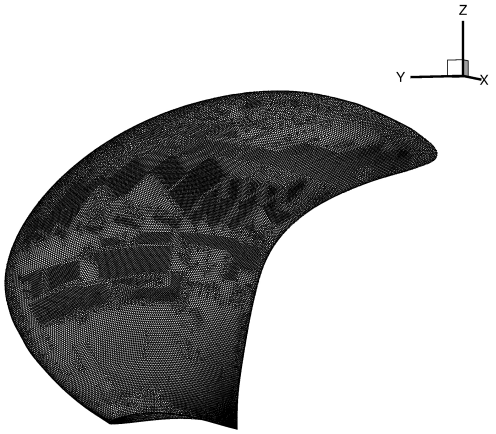

Figure 3: Very fine grids are needed for the RANS simulations of propellers with blunt T.E.s

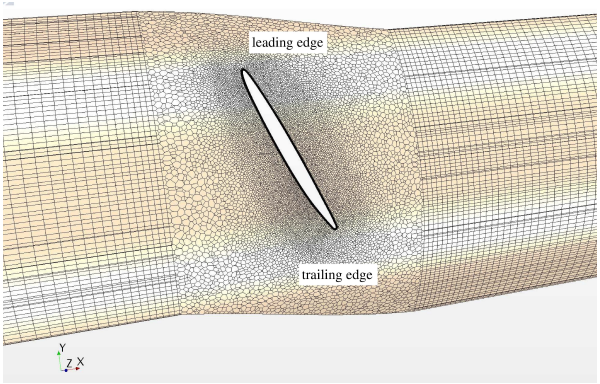

Figure 4: A cylindrical cut at 70% of blade radius to show the O-grids in the RANS model

2.2 The viscous/inviscid interaction (VII) method

In the panel method, the total flow velocity $\overrightarrow{q}$ is decomposed into an incoming flow $\overrightarrow{q_{in}}$ and a propeller-induced flow $\overrightarrow{U_{inv}}$ (the perturbation velocity),

$$\overrightarrow{q} = \overrightarrow{q_{in}} + \overrightarrow{U_{inv}}. \tag{7}$$

$\overrightarrow{U_{inv}}$ can be treated as the potential flow which is governed by the Laplace's equation

$$\overrightarrow{U_{inv}} = \nabla\phi, \quad \nabla^2\phi = 0, \tag{8}$$

where ϕ is the perturbation potential.

The Kutta condition is required which means the velocity must remain finite

$$|\nabla\phi| < \infty \quad \text{at the trailing edge.} \tag{9}$$

By using the Green's identity, (8) can be written in the boundary integral form:

$$\begin{aligned} 2\pi\phi_p = &\iint_{S_H} \left[\phi_p \frac{\partial G(p,p')}{\partial \mathbf{n}_{p'}} - G(p,p')\frac{\partial \phi_p}{\partial \mathbf{n}_{p'}}\right] \mathrm{d}S \\ &+ \iint_{S_W} \Delta\phi_W \frac{\partial G(p,p')}{\partial \mathbf{n}_{p'}} \mathrm{d}S, \end{aligned} \tag{10}$$

where S_H = the surface of the propeller blade; S_W = the surface of the trailing wake; G = the Green's function, which is defined as $1/\mathcal{R}(p,p')$; and $\mathcal{R}$ = the distance between the two points p and p'.

The viscous effect can be considered by coupling the panel method with the boundary layer solvers, known as the viscous/inviscid interaction method. In 2D, the viscous velocity on the ith panel is obtained by

$$\overrightarrow{U_{i,vis}} = \overrightarrow{U_{i,inv}} + \sum_{j=1}^{N+N_W} C_{ij}\sigma_j, \tag{11}$$

where $\overrightarrow{U_{i,inv}}$ = the edge velocity on the ith panel; N and N_W = the number of panels on S_H and S_W, respectively; C_{ij} = the source influence coefficient matrix; and σ_j = the boundary layer source strength on the jth panel. In 3D propellers flows, it is assumed that the boundary layer growth in the span-wise direction is negligible compared with that in the chord-wise direction, so the 2D boundary layer equations are solved strip by strip. However, the 3D influence coefficients are used and the effect of other strips and blades are considered (Kinnas et al., 2012). The viscous velocity on the K^{th} strip is

$$\begin{aligned} \boldsymbol{U_K^{vis}} = &\boldsymbol{U_K^{inv}} + \boldsymbol{D_K}\,\boldsymbol{A_{KK}^{-1}}\boldsymbol{B_{KK}}\,\boldsymbol{\sigma_K} \\ &+ \sum_{J=1,J\neq K}^{MR} \boldsymbol{D_K}\,\boldsymbol{A_{KK}^{-1}}\,\boldsymbol{B_{KJ}}\,\boldsymbol{\sigma_J} \\ &+ \sum_{J=1,J\neq K}^{MR} \boldsymbol{D_K}\,\boldsymbol{A_{KK}^{-1}}\,\boldsymbol{A_{KJ}}\left[\boldsymbol{\phi_J^{inv}} - \boldsymbol{\phi_J^{vis}}\right], \end{aligned} \tag{12}$$

where MR is the number of strips in the span-wise direction, $\boldsymbol{D_K}$ the differentiation matrix with respect to the arc-length on the K^{th} strip, $\boldsymbol{A}$ the dipole induced influence coefficient matrix and $\boldsymbol{B}$ the source induced influence coefficient matrix. The first line of Equation (12) represents the edge velocity plus the influence of the boundary layer sources of the K^{th} strip on the velocity, which is similar to the 2D form in Equation (11). The second line of Equation (12) represents the influence of the boundary layer sources from other strips on the velocity and the last line represents the influence of dipoles from other strips on the velocity. Details of how Equation (12) is derived can be found in Du (2019).

2.3 The 3D flow separation model

2.3.1 Generating the extension from the original geometry

In this paper, a 4-blade open propeller with a blunt T.E., as shown in Figure 5, is used to test the 3D flow separation model. Equation (12) cannot be applied directly to propellers with blunt T.E.s., so an extension is needed. First, MM cylindrical cuts from the blade root to the blade tip are made, each with the same radius, generating MR panels in the span-wise direction in the panel method, where $MR = MM-1$. Half cosine spacing is used so that more panels are concentrated near the blade tip, where the gradient of the propeller loading (circulation) with respect to the radius is expected to be high. In Figure 5, when $i = 1$, the radius of the cut equals the hub radius and when $i = MM$, the radius of the cut equals the blade radius.

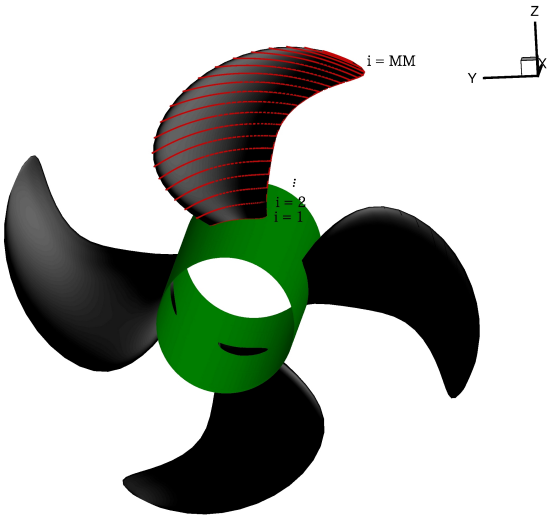

Figure 5: An open propellers with blunt T.E. is used in this study. The total number of the cylindrical cuts from blade hub to tip is MM, and half cosing spacing is used

Each cylindrical cut is transformed into a hydrofoil with a blunt T.E. in the 2D Cartesian system, and extended to a section with a sharp T.E., as shown in Figure 6. Full cosine spacing is used in the chord-wise direction to concentrate more panels near the leading edge and trailing edge and abrupt change in panel sizes between the original part and extended part is avoided. Note that the original section is rotated and scaled based on the chord length of this section, so that the hydrofoil sections with blunt T.E. are placed

between (0, 0) and (1, 0) in the 2D Cartesian system. The extension is built by 2^{nd} order polynomial to ensure that both the geometry and the slope are continuous at Point A and B. If the coordinates of Points A, B and C are given, the extension is uniquely determined by solving the equation set

$$\begin{cases} y_C &= a_1 x_C^2 + b_1 x_C + c_1 \\ y_A &= a_1 x_A^2 + b_1 x_A + c_1 \\ slope_A &= 2a_1 x_A + b_1 \\ y_C &= a_2 x_C^2 + b_2 x_C + c_2 \\ y_B &= a_2 x_B^2 + b_2 x_B + c_2 \\ slope_B &= 2a_2 x_B + b_2 \end{cases}, \tag{13}$$

where x_A, y_A, x_B, y_B, x_C and y_C are coordinates of Points A, B and C, and $slope_A$ and $slope_B$ are known from the original section. The other parameters are the coefficients of the quadratic function and need to be solved.

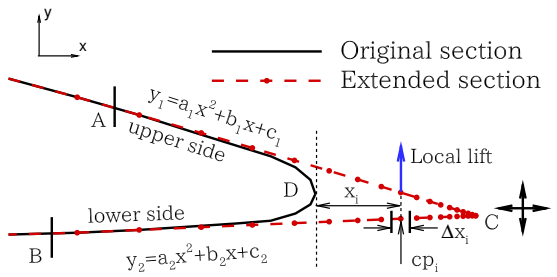

Figure 6: Each hydrofoil section with blunt T.E. is extended to a sharp T.E. section (Points A and B: location where the extended section merges with the original section; Point C: T.E. of the extended section; Point D: T.E. of the original section; Δx_i: length of panel i in x direction; x_i: the moment arm of the local lift with respect to Point D; cp_i: pressure coefficient at the control point of panel i)

In the 2D flow separation model by Du and Kinnas (2018), it is assumed that the pressure in the separated region is constant. Point C is moved in both the horizontal and vertical direction by using the Newton-Secant method until both criteria of zero-lift and zero-moment are satisfied, which is the inner loop of the scheme. In the outer loop, Point A and B are moved along the surface of the foil until they overlap with the flow separation points, where the skin friction c_f is equal to zero with a certain tolerance. Ideally, in the 3D flow separation model, locations of Point A, B and C of all strips need to be determined in a similar way. However, this will introduce too many unknowns, and more importantly, the smoothness of the extended blade with a sharp T.E. cannot be guaranteed.

Based on the experience from the 2D flow separation model, locations of Point A and B (the outer loop) have much less effect on the predicted pressure distribution and forces than the location of Point C. On the other hand, as shown in Figure 6, the shape of the extension is almost unaffected by the location of Point A and B, unless they are very close to the T.E. of the original section. In this study, the location of Point A and B are fixed at 93% of the chord length, based on the skin friction distribution from the RANS simulation.

To guarantee the smoothness of the extension, location of Point C in each strip is determined by using the least square method:

$$\begin{cases} xc(r) &= \alpha_0 + \alpha_1 r + \alpha_2 r^2 + ... + \alpha_m r^m \\ yc(r) &= \beta_0 + \beta_1 r + \beta_2 r^2 + ... + \beta_n r^n \end{cases} \tag{14}$$

where $\alpha_0, \alpha_1, ..., \alpha_m, \beta_0, \beta_1, ..., \beta_n$ are coefficients in the least square method. Let $l = m+n+2$. These l parameters can uniquely determine the shape of the extension and are unknowns to be solved for in the 3D flow separation model. The initial guess of the extension is by assuming that curve AC and BC in all the sections in Figure 6 are straight lines, as shown in Figure 7, and smoothed by using 2^{nd} order polynomial for both xc and yc in Equation (14).

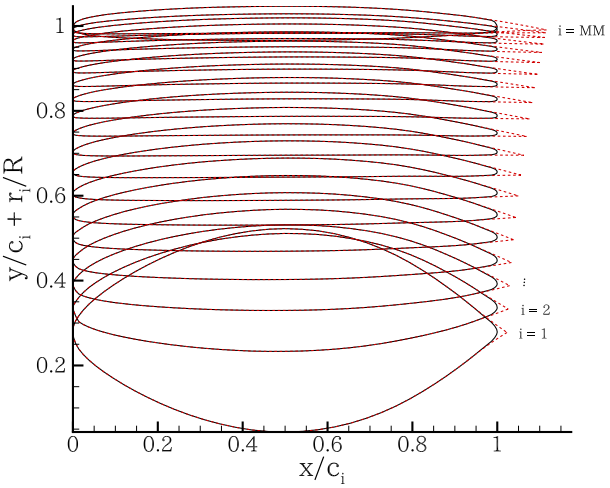

(a) Extension of 2D sections in the initial guess (c_i and r_i: chord length and radius of the section, respectively)

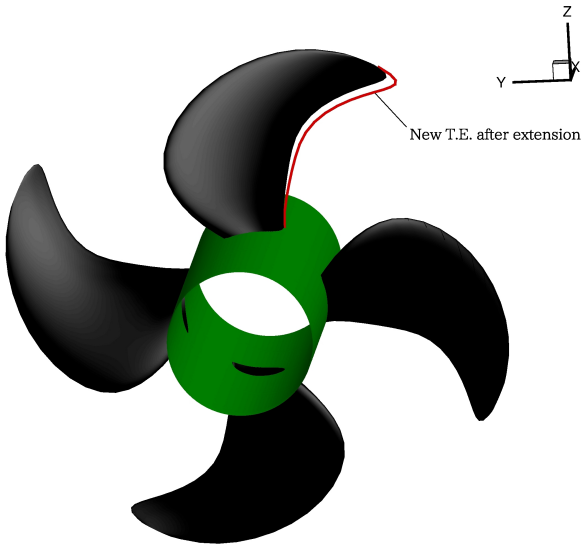

(b) New T.E. after extension in the initial guess

Figure 7: Initial guess of the extension, which is obtained by assuming that both curve AC and BC in Figure 6 are straight lines in all the strips

2.3.2 Model establishment

In this section, the mathematical model for the 3D separation model is established. Define a vector with l elements as $\boldsymbol{\mathcal{X}} = (\alpha_0, \alpha_1, ..., \alpha_m, \beta_0, \beta_1, ..., \beta_n)^T$. Given an initial propeller geometry with blunt T.E. and a vector $\boldsymbol{\mathcal{X}}$, a propeller with sharp T.E. can be uniquely determined. By using a low order panel method, the pressure distribution at each strip of this propeller can be found. The pressure coefficient is defined as

$$c_{p_i} = \frac{p_i - p_\infty}{\frac{1}{2}\rho v_\infty^2}, \tag{15}$$

where p_∞ = the pressure at far upstream; and v_∞ = the velocity at far upstream, assumed to be uniform.

Similar to the 2D flow separation model, it is assumed that the pressure in the extended region of each strip is constant, which leads to the zero-lift and zero-moment criteria. The local lift and local moment downstream of the extension of jth panel in the span-wise direction is defined as (only the extended part downstream of Point D in Figure 6 is considered)

$$\begin{cases} \Delta F_j &= \dfrac{\sum\limits_{lower,upper}\sum\limits_{i} c_{p_i} \times \Delta x_i}{\sum\limits_{lower,upper}\sum\limits_{i} \Delta x_i} \times \Delta r_j \\ \Delta M_j &= \dfrac{\sum\limits_{lower,upper}\sum\limits_{i} c_{p_i} \times \Delta x_i \times x_i}{\sum\limits_{lower,upper}\sum\limits_{i} \Delta x_i \times x_i} \times \Delta r_j \end{cases} \tag{16}$$

where Δr_j is the length of the panel in the span-wise direction. Since there are MR panels, there are $2 \times MR$ outputs from each extension. Define a vector for these outputs:

$$\boldsymbol{G} = (\Delta F_1, \Delta F_2, ..., \Delta F_{MR}, \Delta M_1, \Delta M_2, ...\Delta M_{MR})^T$$

The 3D flow separation model can be rephrased as: find vector $\boldsymbol{\mathcal{X}}$, so that all the elements in vector $\boldsymbol{G}$ are zero. There are two methods to solve this problem.

2.3.3 Newton-Secant method

In this method, the new vector $\boldsymbol{g}$ of dimension l is derived by least square regression from $\boldsymbol{G}$ so that a square shape Jacobian matrix can be generated in the Newton-Secant method:

$$\begin{cases} \Delta F(r) &= \gamma_0 + \gamma_1 r + \gamma_2 r^2 + ... + \gamma_m r^m \\ \Delta M(r) &= \gamma_{m+1} + \gamma_{m+2} r + \gamma_{m+3} r^2 + ... + \gamma_l r^n \\ \boldsymbol{g} &= (\gamma_1, \gamma_2, ..., \gamma_l)^T \end{cases} \tag{17}$$

where $\boldsymbol{g}$ is a function of $\boldsymbol{\mathcal{X}}$, and Newton-Secant method is used to find the root $\boldsymbol{\mathcal{X}}$ for the function $\boldsymbol{g} = 0$.

2.3.4 Optimization problem

There are some limitations in the Newton-Secant method. First, it requires the derivatives of function $\boldsymbol{g}$ with respect to $\boldsymbol{\mathcal{X}}$ to exist, which might not always be true. Second, this method might encounter convergence problems, or even converge to wrong answers if the initial guess is far away from the final solution.

This mathematical model can also be solved by regarding it as an optimization problem. First, define $g_0 = ||\boldsymbol{g}||$, where $||\boldsymbol{g}||$ is the norm of vector $\boldsymbol{g}$. The optimization problem is defined as

$$\begin{aligned} &minimize \quad g_0(\boldsymbol{\mathcal{X}}) \\ &subject\ to \quad h_i(\boldsymbol{\mathcal{X}}) \leq 0 \quad i = 1, 2, \ldots, q \end{aligned} \tag{18}$$

where $h_i(\boldsymbol{\mathcal{X}})$ is the inequality constraints so that the extended geometry is not abnormal. One benefit is that there are many optimization methods to find the solution, some of which do not require the derivatives to exist, and we can choose one that best fits the character of this problem.

3 RESULTS AND DISCUSSION

3.1 The Reynolds-Averaged Navier-Stokes method

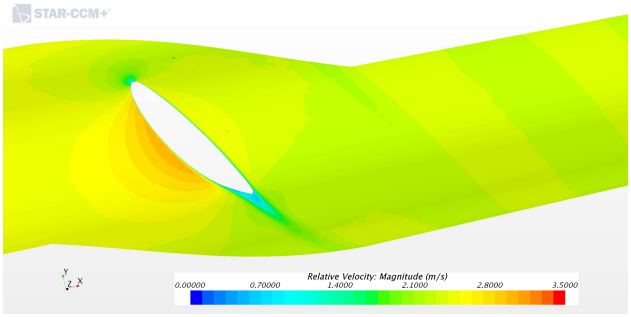

(a) $r/R = 0.4$

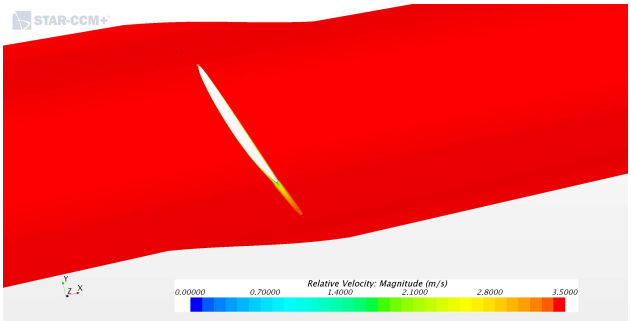

(b) $r/R = 0.7$

Figure 8: Relative velocity magnitude at different sections from the RANS simulation (plotted with $V_s = 1m/s$ and $J_s = 0.579$). Note the low velocity region downstream of the blunt T.E. due to flow separation

The relative velocity magnitude contour plots at two sections with constant radii are shown in Figure 8 at $J_s = 0.579$. The velocity downstream of the blunt T.E. is low due to the flow separation. The wall distance $y+$ for this simulation is shown in Figure 9. The pressure coefficients and computational efficiency will be shown in later sections with results from the 3D flow separation model.

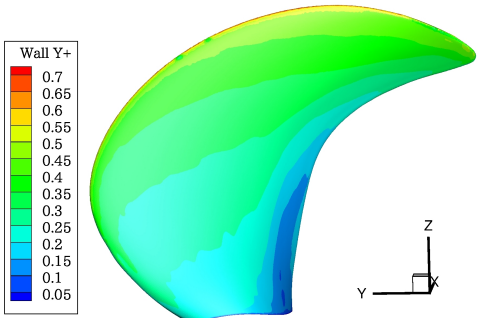

Figure 9: Wall $y+$ in the RANS simulation for the propeller with blunt T.E.

The open water characteristics of this propeller are predicted by the RANS method at a range of advance ratios, which are based on the advance speed and rate of revolutions in the open water test. The viscosity in the RANS simulation is based on the water temperature during the experiment.

3.2 The viscous/inviscid interaction (VII) method

In the 3D flow separation model, propellers with sharp T.E.s are generated for each $\mathcal{X}$. The panel method coupled with a 2D integral boundary layer solver, known as the viscous/inviscid interaction method, is used to find the pressure distribution at different radii of each geometry. It is necessary to test the accuracy of the VII method with known experimental data. Du and Kinnas (2019) showed that for a five-blade propeller with sharp T.E. (Propeller 5168), the VII method greatly improves the correlation of the predicted thrust and torque with the experimental data, compared with the pure panel method without the boundary layer corrections. In this study, the full wake alignment (FWA) scheme is used to predict the location of the trailing wake, developed by Tian and Kinnas (2012).

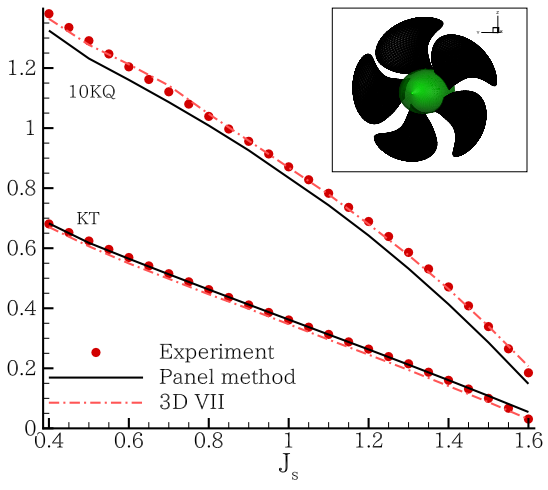

Figure 10: The open water characteristic of a propeller with sharp T.E., taken from Du and Kinnas (2019)

3.3 The 2D flow separation model

The 2D flow separation model was applied to a bare duct with round T.E. section (Du and Kinnas, 2018). The interaction between the propeller and the duct is neglected so the problem is simplified to two-dimensional, and the axisymmetric sources are used in the viscous/inviscid interaction method. The pressure distribution agrees well with those from the RANS method, as shown in Figure 12.

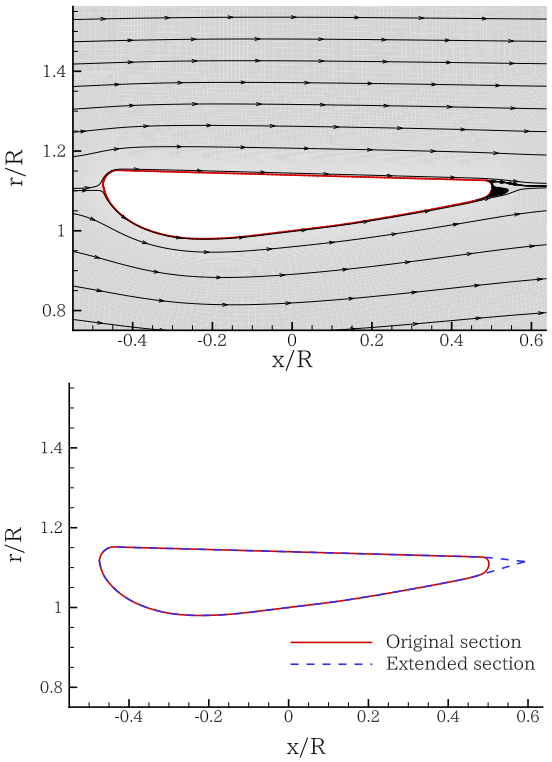

Figure 11: Streamlines around a duct with a round T.E., note that the local flow separation downstream of the T.E. (predicted by the steady axisymmetric RANS simulation) is replaced by an extension in the flow separation model

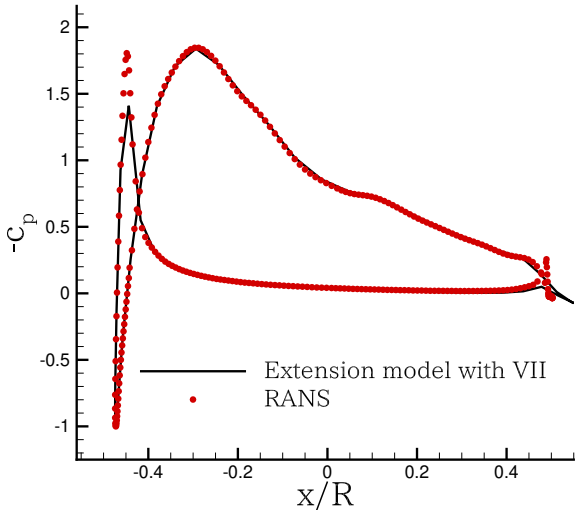

Figure 12: The pressure distribution from the 2D flow separation model and the RANS method in a bare duct with a round T.E., $Re = 1.0 \times 10^6$ (Du and Kinnas, 2018)

3.4 The 3D flow separation model

Based on the results of the 2D flow separation model, yc (location of Point C in the vertical direction) has a stronger

effect on the pressure distribution than xc, because y_C affects the camber of the section, which is directly related with the propeller loading. In this paper, xc and yc in Equation (14) are approximated by 2^{nd} order polynomial in the least square method from the initial guess shown in Figure 7 but only yc is determined by the model. xc is determined only once from the initial guess (by assuming curve AC and BC to be straight lines in Figure 6) and then kept constant throughout this study. It should be noted that different order of polynomial for yc will affect the extended geometry, and the local lifts are also affected. As shown in Figure 13, similar local lift distributions are observed by using 2^{nd} order and 3^{rd} polynomials to approximate the initial guess but yc approximated by higher orders will lead to the unsmoothness in the distribution. In this paper, 2^{nd} order polynomials are used for yc distribution. For a complete study of higher order polynomials and the effect of xc on the results, please refer to Du (2019).

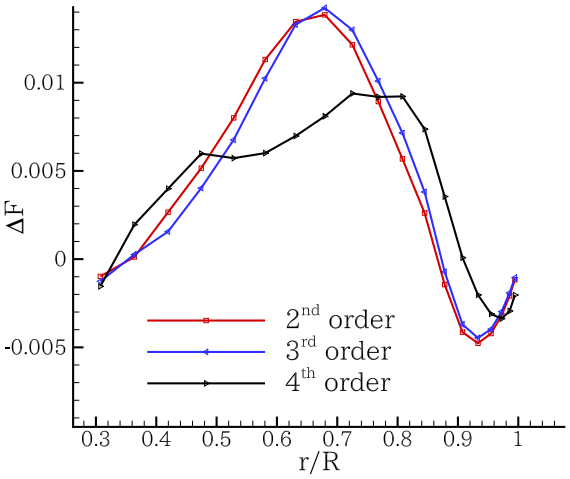

Figure 13: The local lift distribution of the initial guess, approximated by using different orders of polynomial for yc

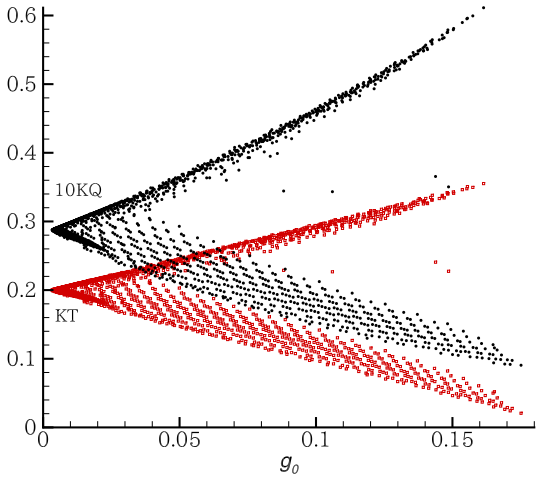

Figure 14: The thrust, torque and g_0 of all extended propeller blades in the global search in the optimization algorithm ($J_s = 0.579$)

The Newton-Secant method fails to converge for the propeller case at this stage. Consequently, the 3D flow separation is solved as an optimization problem and a global search method is used to find the solution $\mathcal{X}$. Some inequality constraints are applied on $\mathcal{X}$ so that the extended geometry is reasonable. In this paper, the infinity norm is used, i.e., $g_0 = ||\boldsymbol{g}||_\infty$.

As shown in Figure 14, the location of the T.E. has a strong effect on the forces of the propeller. At $J_s = 0.579$, the converged KT (i.e., the KT corresponding to the minimum g_0) is about 0.2, but the KTs of all extensions are in the range of 0.02 to 0.36. The converged 10KQ is about 0.29, but the 10KQs of all extensions are in the range of 0.1 to 0.6. More importantly, the differences between the forces of an extended blade and the converged forces almost linearly increase as g_0 becomes larger. At this advance ratio, the maximum g_0 is about 50 times bigger than the minimum g_0 for all the searched blade extensions. To conclude, it is critical to find the extension with minimum g_0 so that the local lifts and moments are close to zero.

In this paper, there are two stages in the 3D flow separation model. In the first stage, several rounds of searches are conducted until the changes in $\mathcal{X}$ fall under certain pre-defined tolerances. Each propeller with a sharp trailing edge is solved by the panel method with a fast wake alignment scheme (PSF-2 type alignment). It should be noted that in this stage, the panel method is not coupled with the boundary layer solver and the inviscid pressure is used to calculate the local lifts and local moments. In this way, the computational time is greatly reduced, and the stability of the numerical scheme is also improved because the boundary layer solver might fail to converge for some blade sections. After the extension is found, the propeller is solved by the panel method with the full wake alignment scheme (more accurate but more time-consuming) with the boundary layer corrections, which is regarded as the second stage of the current method.

The pressure distributions from the current method and from the RANS method are shown in Figure 15. Compared with results from the 2D flow separation model in Figure 12, the correlation is not as good. On one hand, predicting the three-dimensional flow separations for propellers with blunt T.E.s is much more challenging than predicting the flow separations in two-dimensional for hydrofoils and propeller ducts, with an increased number of unknowns and more assumptions in the model.

On the other hand, the results from RANS might be questionable because modeling propellers with blunt T.E. is also challenging for the RANS method due to the fact that only a short part in the wake region can be modeled with sufficiently fine grids. In 2D RANS simulations very fine grids can be afforded at a long distance downstream of the blunt T.E. in order to capture accurately a long part of the trailing wake. However, due to limitations in building the grids around propellers with blunt T.E., a sufficient grid resolution in the trailing wake is very hard to achieve even with a prohibitively excessive number of cells.

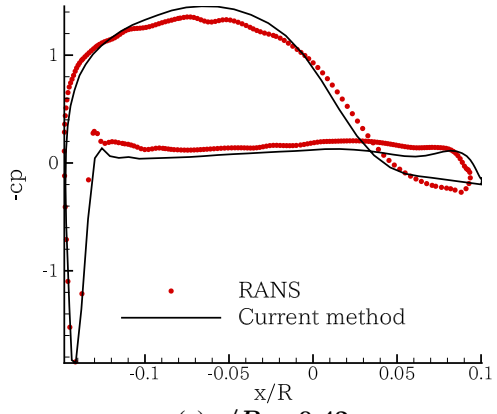

(a) $r/R = 0.42$

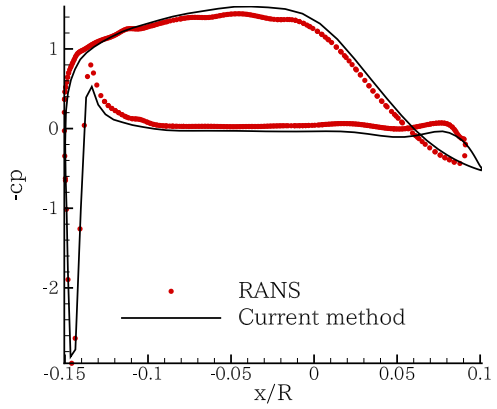

(b) $r/R = 0.53$

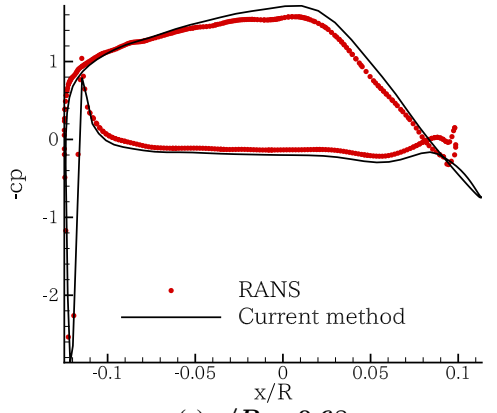

(c) $r/R = 0.68$

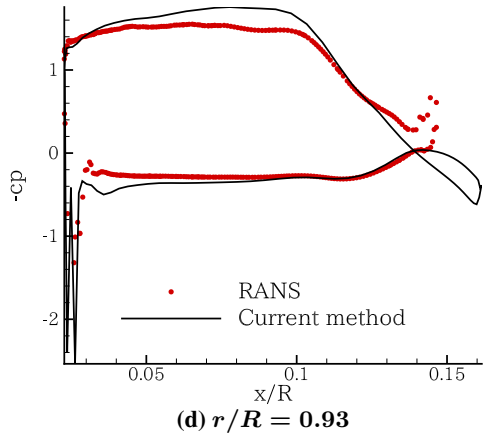

(d) $r/R = 0.93$

Figure 15: Pressure distributions from the 3D flow separation model and the RANS simulations

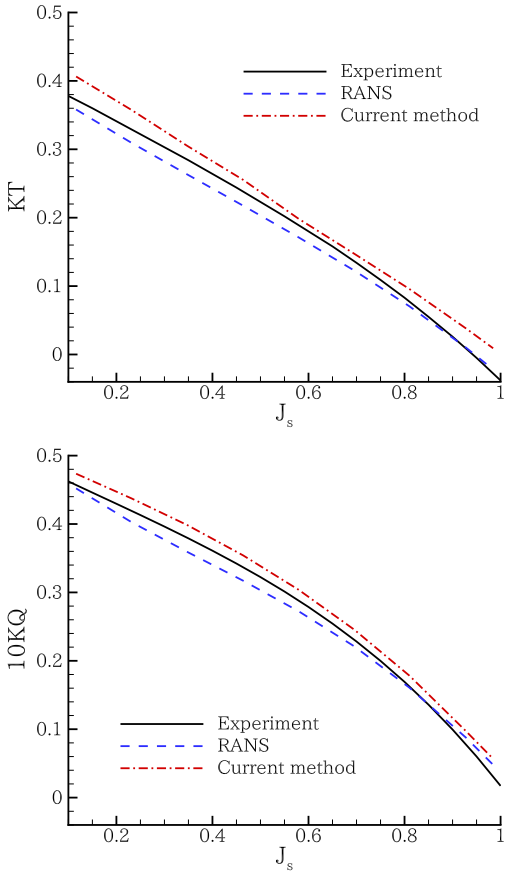

Figure 16: The open water characteristics predicted from the current method, RANS, and the experimental measurements

The open water characteristics of the propeller with a blunt T.E. from the current method and RANS simulations are compared with the experimental measurements, as shown in Figure 16. The inflow is uniform, and at each advance ratio, the Reynolds number (defined by the propeller diameter) is the same among the current method, the RANS simulations and the experiment. At $J_s = 0.579$, the RANS method under-predicted KT by 10.3% and under-predicted 10KQ by 6.06%. At the same advance ratio, the present method over-predicted KT by 3.88% and over-predicted 10KQ by 4.75%.

3.5 CPU time

Compared with the RANS method, the 3D flow separation model does not require as many computational resources and takes a shorter time in the calculation, not to mention the time for pre-processing and post-processing. An overall comparison of the computational efficiency of these two methods is shown in Table 2. All the simulations were done on the clusters of TACC (Texas Advanced Computing Center) by using the Intel Xeon E5-2680 2.7GHz processor. In the RANS method, only the simulation time was counted. In the current method, the first stage is labeled as *search* and the second stage is labeled as *FWA/BL* (full wake alignment with boundary layer corrections). It should be noted that by using different methods in this model, the time for the first stage might be greatly reduced. In this paper, the global search scheme is used, which might be the least efficient option.

Table 2: The computational efficiency of the current method and the RANS method (only the simulation time was counted)

$J_s = 0.579$		Number of CPUs	Wall clock time
RANS		64	118.2 min
3D flow separation model	Search	48	18.1 min
	FWA/BL	48	4.2 min
	Total	-	22.3 min

4 CONCLUSIONS

In this paper, a 3D flow separation model is proposed so that the viscous/inviscid interaction method can be used to predict the flows around propellers with blunt T.E.s. It is assumed that the pressure in the separated region is constant, and a mathematical model is established. Different methods are proposed to solve this model. After the extension is found, the propeller is solved in the viscous/inviscid interaction method, which couples a panel method with a boundary layer solver, and the full wake alignment scheme is used.

From this study, it is found that correct extensions are critical to accurately predict forces of the propeller. When the local lift and local moment from the extension are close to zero, i.e., when the criteria in the current method are satisfied, the predicted thrust and torque converges to a value close to the experimental data. However, when the criteria are not satisfied, the predicted forces might be very different from those in the experiment.

Compared with the RANS method, the present method requires shorter computational time and fewer computational resources, and the predicted open water characteristics agree well with the experimental measurements. To conclude, this model can be a useful tool in designing and analyzing propellers with blunt T.E.s.

5 FUTURE WORK

In the future, the computational time can be greatly reduced by using more computationally efficient methods to find the extension. In this paper, the extension length (xc) is fixed and the location in the direction perpendicular to the extension in each section (yc) is determined by the model. A study in the 2D flow separation model shows that yc has a stronger effect on the pressure distributions and forces. In the future, a complete study for xc and higher order polynomials in $\mathcal{X}$ will be included in this model, and locations to start the extension will be determined from the flow separation points.

6 ACKNOWLEDGEMENTS

Support for this research was provided by the US Office of Naval Research (Grant Number N00014-14-1-0303 and N00014-18-1-2276; Dr. Ki-Han Kim) partly by Phase VIII of the Consortium on Cavitation Performance of High Speed Propulsors.

REFERENCES

Drela, M. (1989). 'XFOIL: an analysis and design system for low Reynolds number airfoils'. In Low Reynolds number aerodynamics, pages 1–12. Springer.

Du, W. (2019). 'Application of the Three-Dimensional Viscous/Inviscid Interaction Method on Predicting the Performance of Propulsors with Blunt Trailing Edges'. PhD thesis, The University of Texas at Austin.

Du, W. and Kinnas, S. A. (2018). 'A flow separation model for hydrofoil, propeller and duct sections with blunt trailing edges'. Journal of Fluid Mechanics, 861:180–199.

Du, W. and Kinnas, S. A. (2019). 'Applying 3D Viscous/Inviscid Interaction Method to Predict Flows Around Wings and Propellers'. In SNAME 24th Offshore Symposium. The Society of Naval Architects and Marine Engineers.

Greeley, D. S. and Kerwin, J. E. (1982). 'Numerical methods for propeller design and analysis in steady flow'. Transactions of Society of Naval Architects and Marine Engineers, 90:415–453.

Hufford, G. S., Drela, M., and Kerwin, J. E. (1994). 'Viscous flow around marine propellers using boundary-layer strip theory'. Journal of Ship Research, 38:52–62.

Kerwin, J. E. and Lee, C.-S. (1978). 'Prediction of steady and unsteady marine propeller performance by numerical lifting-surface theory'. In Transactions of Society of Naval Architects and Marine Engineers.

Kim, S., Kinnas, S. A., and Du, W. (2018). 'Panel method for ducted propellers with sharp trailing edge duct with fully aligned wake on blade and duct'. Journal of Marine Science and Engineering, 6(3):89.

Kinnas, S. A., Yu, X., and Tian, Y. (2012). Prediction of propeller performance under high loading conditions with viscous/inviscid interaction and a new wake alignment model. In Proceedings of the 29th Symposium on Naval Hydrodynamics, Gothenburg, Sweden, pages 26–31.

Milewski, W. M. (1997). 'Three-dimensional viscous flow computations using the integral boundary layer equations simultaneously coupled with a low order panel method'. PhD thesis, Massachusetts Institute of Technology.

Reynolds, O. (1894). 'On the dynamical theory of incompressible viscous fluids and the determination of the criterion'. Philos. Trans. R. Soc. London Ser. A, 186:123–164.

Spalart, P. and Allmaras, S. (1992). 'A one-equation turbulence model for aerodynamic flows'. In 30th aerospace sciences meeting and exhibit, page 439.

Sun, H. and Kinnas, S. (2008). 'Performance prediction of cavitating water-jet propulsors using a viscous/inviscid interactive method'. Transactions of Society of Naval Architects and Marine Engineers, 116:166–181.

Tian, Y. and Kinnas, S. A. (2012). 'A wake model for the prediction of propeller performance at low advance ratios'. Int. J. Rotating Machinery, 2012.